

Studying reionization with the next generation of Ly α emitter surveys

H. Jensen^{1*}, M. Hayes^{1,2,3}, I. T. Iliev⁴, P. Laursen⁵, G. Mellema¹, E. Zackrisson¹

¹*Dept. of Astronomy and Oskar Klein Centre, Stockholm University, AlbaNova, SE-10691 Stockholm, Sweden*

²*Université de Toulouse; UPS-OMP; IRAP; Toulouse, France*

³*CNRS; IRAP; 14, avenue Edouard Belin, F-31400 Toulouse, France*

⁴*Astronomy Centre, Department of Physics & Astronomy, Pevensey II Building, University of Sussex, Falmer, Brighton BN1 9QH, UK*

⁵*Dark Cosmology Centre, Niels Bohr Institute, University of Copenhagen, Juliane Maries Vej 30, 2100 Copenhagen, Denmark*

6 December 2024

ABSTRACT

We study the prospects for constraining the ionized fraction of the intergalactic medium (IGM) at $z > 6$ with the next generation of large Ly α emitter surveys. We make predictions for the upcoming Subaru Hyper Suprime-Cam (HSC) Ly α survey and a hypothetical spectroscopic survey performed with the James Webb Space Telescope (JWST). Considering various scenarios where the observed evolution of the Ly α luminosity function of Ly α emitters at $z > 6$ is explained partly by an increasingly neutral IGM and partly by intrinsic galaxy evolution, we show how clustering measurements will be able to distinguish between these scenarios. We find that the HSC survey should be able to detect the additional clustering induced by a neutral IGM if the global IGM neutral fraction is greater than ~ 20 per cent at $z = 6.5$. If measurements of the Ly α equivalent widths (EWs) are also available, neutral fractions as small as 10 per cent may be detectable by looking for correlation between the EW and the local number density of objects. In this case, if it should turn out that the IGM is significantly neutral at $z = 6.5$ and the intrinsic EW distribution is relatively narrow, the observed EWs can also be used to construct a map of the locations and approximate sizes of the largest ionized regions. For the JWST survey, the results appear a bit less optimistic. Since such surveys probe a large range of redshifts, the effects of the IGM will be mixed up with any intrinsic galaxy evolution that is present, making it difficult to disentangle the effects. However, we show that a survey with the JWST will have a possibility of observing a large group of galaxies at $z \sim 7$, which would be a strong indication of a partially neutral IGM.

Key words: cosmology: dark ages, reionization, first stars—methods: numerical

1 INTRODUCTION

The Epoch of Reionization (EoR) is the time period in the history of the Universe when the first sources of light formed and ionized the intergalactic medium (IGM). Observations of quasar spectra indicate that this process must have been largely completed around $z \approx 6$ (Fan et al. 2006), but the exact details beyond this redshift—both in terms of the timing of reionization and the sources responsible—are still not well known. Some additional observational constraints come from the polarisation of the cosmic microwave background (Komatsu et al. 2011; Larson et al. 2011) and temperature measurements (Theuns et al. 2002; Raskutti et al. 2012). However, these observations are still consistent with a great range of reionization scenarios (Mitra, Choudhury & Ferrara 2012).

During the past decade, Ly α emitters have attracted considerable attention as potential probes of the latest stages of the EoR (e.g. Hu et al. 2002; Malhotra & Rhoads 2004; Ota et al. 2008; Stark et al. 2010; Ouchi et al. 2010; Hu et al. 2010; Kashikawa et al. 2011; Pentericci et al. 2011; Caruana et al. 2013; Treu et al. 2013; Pentericci et al. 2014; Tilvi et al. 2014). Since Ly α photons are resonantly scattered by neutral hydrogen, the Ly α luminosity from a galaxy is suppressed if the galaxy is surrounded by a neutral IGM. Therefore, we would expect the statistics and number counts of Ly α emitters to change at redshifts where reionization is not yet completed. In principle, it should be possible to use this change to measure how neutral the IGM is at a certain redshift.

While some earlier studies saw no evidence of evolution in the Ly α luminosity function of Ly α emitters at redshifts $\gtrsim 6$ (Malhotra & Rhoads 2004; Tilvi et al. 2010), in the past few years several observational studies have established that there is in fact a rapid

* hannes.jensen@astro.su.se

evolution in the population of Ly α emitters. Ouchi et al. (2010) and Kashikawa et al. (2011) showed that the luminosity function drops in amplitude between $z = 5.7$ and $z = 6.5$, after being roughly constant in the interval $3 < z < 5.7$. In a similar vein, Stark et al. (2010), Pentericci et al. (2011, 2014), Treu et al. (2013), Caruana et al. (2013) and Faisst et al. (2014) all find that the fraction of drop-out selected galaxies that show Ly α emission decreases rapidly between $6 < z < 7$. It is tempting to view these observations as evidence of an increase in the IGM neutral fraction at $z > 6$.

However, simulations that try to quantify how high the IGM neutral fraction needs to be to account for this evolution at $z > 6$ typically require very late and rapid reionization scenarios, with neutral fractions as high as 40 per cent at $z = 6.5$ (Dijkstra, Mesinger & Wyithe 2011; Pentericci et al. 2011; Jensen et al. 2013). Such high neutral fractions are hard to justify physically, and seem incompatible with measurements of the IGM temperature (Raskutti et al. 2012) and Ly α line profile measurements (Ouchi et al. 2010). Several ways of easing this tension between simulations and observations have been proposed, including intrinsic evolution in the Ly α emitters (Dayal & Ferrara 2011; Hutter et al. 2014; Dijkstra et al. 2014), sample variance in the observations (Taylor & Lidz 2014) and the presence small-scale high-density structures (Bolton & Haehnelt 2013).

While measurements of the luminosity function and the Ly α emitter fraction cannot distinguish between intrinsic evolution and IGM evolution, the additional clustering of Ly α emitters due to a partially ionized IGM could be used as a much more robust probe of the ionization state of the IGM (McQuinn et al. 2007a; Ouchi et al. 2010). As seen in Jensen et al. (2013), this method requires sample sizes of several thousand objects to put meaningful constraints on reionization. Such large samples are not available today, but upcoming observations with the Hyper-Suprime Cam (HSC) on the Subaru telescope, will observe some 5500 narrow-band selected Ly α emitters over a total of 30 deg² at $z = 6.5$ (M. Ouchi 2013, private communication). Furthermore, the James Webb Space Telescope (JWST) will perform deep spectroscopic surveys of Ly α emitters at high redshifts. However, to date, few systematic investigations have been performed regarding what new information about reionization that will be possible to extract from these observations, besides better measurements of quantities like the Ly α luminosity function and Ly α emitter fraction.

This paper is a first step towards providing such study. We investigate the extent to which the next generation of large-field Ly α emitter surveys—such as the HSC survey—and deep spectroscopic surveys—for example with the JWST—may be able to distinguish between intrinsic galaxy evolution and a neutral IGM, focusing mainly on clustering measurements, which are beyond the reach of today’s surveys. Furthermore, we explore the possibilities of using such large Ly α samples to perform “bubble-mapping”, i.e. determining the positions and shapes of the largest H II regions.

The paper is structured as follows: in section 2 we describe our simulations and physical assumptions. We also discuss how the clustering of Ly α emitters is affected by a partially neutral IGM and how this clustering can be quantified. In section 3, we present our predictions, first for the HSC survey and then for the JWST survey. Here, we also comment briefly on the recent observational results of Pentericci et al. (2014) and Tilvi et al. (2014). Finally, in section 4, we summarize and discuss our results.

For the simulations, we have assumed a flat Λ CDM model with $(\Omega_m, \Omega_b, h, n, \sigma_8) = (0.27, 0.044, 0.7, 0.96, 0.8)$, consistent with the 9 year WMAP results (Hinshaw et al. 2013).

2 METHODS

Our goal is to produce mock observational samples that incorporate different combinations of intrinsic galaxy evolution and evolution of the IGM ionized fraction. To do this, we start with a large cosmological simulation of the IGM. We then assign intrinsic Ly α emission properties to the dark matter haloes in the simulation and calculate the Ly α emission through the IGM at various global ionized fractions. The methods used here are essentially identical to those described in detail in Jensen et al. (2013), although we use a much larger simulation volume here.

2.1 Simulations of the IGM

To simulate the reionization of the IGM we start with a $(607 \text{ cMpc})^3$ N -body simulation produced with the CUBEP³M code (Harnois-Déraps et al. 2013). Based on PMFAST (Merz, Pen & Trac 2005), CUBEP³M works by calculating gravitational forces on a particle-to-particle basis at short distances, and on a grid at long distances. For this simulation, we used 5488³ particles on a 10976³ grid, which was eventually down-sampled to 504³ grid points. The particle mass was $5 \times 10^7 M_\odot$.

After identifying haloes with a spherical-overdensity halo finder, we simulate the reionization of the IGM using the C²-RAY code (Mellema et al. 2006). C²-RAY is a photon-conserving ray-tracing code that uses short-ray characteristics to solve the equation for the evolution of the ionization fraction of hydrogen by iterating over all sources and grid points until convergence.

In this simulation, we assigned all haloes an ionizing flux \dot{N}_γ proportional to the halo mass M_h :

$$\dot{N}_\gamma = g_\gamma \frac{M_h \Omega_b}{(10 \text{ Myr}) \Omega_m m_p}, \quad (1)$$

where m_p is the proton mass and g_γ is a source efficiency coefficient that effectively incorporates the star formation efficiency, the initial mass function and the escape fraction. The haloes identified with the halo finder had masses down to $10^9 M_\odot$; these were assigned a source efficiency of $g_\gamma = 1.7$. In addition to this, we also added smaller sources with M_h down to $10^8 M_\odot$ using a subgrid recipe (Ahn et al., in preparation). These were assumed to have a $g_\gamma = 7.1$, to account for a lower metallicity and a more top-heavy initial mass function. On the other hand, since small haloes lack the gravitational potential to keep accreting matter in a highly ionized environment (e.g. Iliev et al. 2007), these low-mass sources were turned off when the local ionization fraction exceeded 10 per cent. For more information about these codes and this particular simulation run and the assumptions behind the simulation parameters, see Iliev et al. (2014).

2.2 Simulations of Ly α emitters

The next step is to simulate the observed Ly α emission from the haloes from the previous step. We use the same two-step model as in Jensen et al. (2013), where we model the Ly α line shape emerging from the circum-galactic medium, $J_{\text{em}}(\lambda)$, using a recipe based on high-resolution simulations, and then trace sight-lines through the IGM, calculating the optical depth due to scatterings out of the line-of-sight. The division between the circum-galactic and extra-galactic parts was taken to be at $1.5r_{\text{vir}}$, where r_{vir} is the virial radius of the halo, motivated by the simulations of Laursen, Sommer-Larsen & Razoumov (2011).

The line shape recipe we use is the Gaussian-minus-Gaussian

(GmG) model introduced in Jensen et al. (2013). This recipe is a fit to high-resolution hydrodynamical+Ly α radiative transfer simulations. It gives double-peaked line shapes that are symmetric on the blue and red sides of the line centre, and widen as the halo mass increases. Such a line shape gives a slightly weaker dependence on IGM neutral fraction for the IGM transmission of Ly α than models where a big part of the emission comes from the line centre (e.g. Dijkstra, Mesinger & Wyithe 2011; Jensen et al. 2013). This will tend to make our predictions here somewhat on the conservative side. In reality, far from all observed Ly α lines show a double-peaked structure. However, at the redshifts considered here, the red peak will almost always be absorbed by the IGM, and will only affect the normalization of the intrinsic Ly α luminosity (see below). For a more in-depth discussion about other line-shape models, both analytical and simulated, see Jensen et al. (2013).

For the IGM part of the Ly α radiative transfer, we use the same modified version of IGMTRANSFER (Laursen, Sommer-Larsen & Razoumov 2011) as described in Jensen et al. (2013). The optical depth for Ly α photons is summed over all cells along the sight-line:

$$\tau(\lambda) = \sum_i^{\text{cells}} n_{\text{HI},i} \sigma_{\text{Ly}\alpha}(\lambda + \lambda v_{||,i}/c) \Delta r, \quad (2)$$

where Δr is the length of each step, $n_{\text{HI},i}$ is the local neutral hydrogen density, $\sigma_{\text{Ly}\alpha}$ is the neutral hydrogen cross section to Ly α scattering and $v_{||,i}$ is the gas velocity component of the cell along the line of sight, including the Hubble flow. Using this method, we calculate the transmission of Ly α through the IGM for sightlines along the three coordinate axes for all haloes with $M_h > 10^{10} M_\odot$. By multiplying the line profile with $\exp(-\tau_\lambda)$ we then get the observed line profile. The fraction T_α of Ly α photons that are transmitted through the IGM is then:

$$T_\alpha = \frac{\int J_{\text{em}}(\lambda) \exp(-\tau_\lambda) d\lambda}{\int J_{\text{em}}(\lambda) d\lambda}. \quad (3)$$

A weakness of this method is that the division between the circum-galactic and extragalactic part (which we put at 1.5 virial radii) in reality depends on the amount of neutral hydrogen. While our value appears reasonable for a fairly ionized medium, it is probably less realistic for a more neutral case. A more proper approach would be to carry out the full radiative transfer of Ly α for every galaxy out to a distance where no more photons scatter into the line-of-sight. However, this would require a very high resolution and would be very computationally expensive. Here, we therefore use the same division and line model for all ionization fractions, but note that this may cause us to underestimate the effects of the IGM somewhat.

We also need a model for the intrinsic Ly α and UV continuum luminosities of the galaxies (here, we use the word *intrinsic* to mean the luminosity of the light as it exits the galaxies at $1.5 r_{\text{vir}}$). Since we are interested only in the evolution of the observables due to the IGM neutral fraction, we make no attempt to construct a physically motivated model for the intrinsic properties. Instead, we simply calibrate the luminosities to observations at $z = 5.7$.

In our model for the intrinsic properties, each dark matter halo with mass M_h from the N -body simulations is assigned a Ly α luminosity randomly drawn from a log-normal distribution with a standard deviation of $\sigma = 0.4$ dex and a mean that is proportional to M_h . The normalisation of the luminosities is simply a fit to observations and has no influence on our results, since we are only interested in the changes of various properties. For example, the normalisation of the intrinsic Ly α luminosity is degenerate with

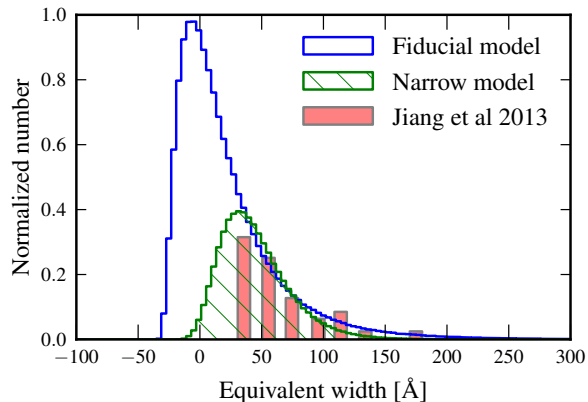


Figure 1. The probability density function for our two assumed EW distributions, compared with the observations by Jiang et al. (2013). For the rest of the paper, results are shown for the fiducial model, unless stated otherwise. The distributions shown here are those which would be observed assuming 50 per cent transmission of Ly α through the IGM.

our line shape model. Had we assumed a line shape with no blue peak, the intrinsic Ly α luminosities would have been a factor 2 lower. The change in luminosity with an increasing IGM neutral fraction, however, would be the same.

The more important quantity here is σ , which gives us the amount of random scatter in the distributions of luminosities. More random scatter leads to a weaker correlation between galaxy mass and luminosity, which, as we shall see, makes methods that rely on the spatial clustering of Ly α emitters less viable for constraining reionization. The value of σ was chosen based on the same set of high-resolution simulations that we used for the Ly α line shape model. As we shall see in the next section, our Ly α luminosity model results in luminosity functions with rather shallow slopes compared to observations. Since higher values of σ give shallower slopes, this indicates that if anything, we are over-estimating the random scatter in the Ly α luminosities. This would make our predictions for clustering somewhat conservative, since more randomness tends to make luminosity-selected galaxies appear less clustered.

For the Ly α EW—essentially the ratio between Ly α and UV continuum luminosity—we use a similar approach, assigning each dark matter halo an EW drawn from a probability distribution (for the remainder of the paper, we will use “EW” to mean restframe EW). The exact shape of the intrinsic EW distribution at $z = 6.5$ is not well known, but observations from lower redshifts suggest that a log-normal distribution is reasonable (e.g. Reddy & Steidel 2009). Our fiducial EW distribution is shown as the blue histogram in Fig. 1. In this model, 65 per cent of all galaxies have Ly α EWs lower than 25 \AA , which is consistent with the EW distribution of Lyman-break selected galaxies observed by Jiang et al. (2013). Later on in the paper, we also consider a more narrow EW model, shown as a green histogram in Fig. 1. In the narrow model, approximately 25 per cent of all galaxies have a Ly α EW lower than 25 \AA . This is only marginally consistent with the least luminous galaxies of Stark et al. (2010), and thus represents a bit of an extreme case. For the rest of the paper, if nothing else is stated, results are shown for the fiducial EW model. For both models, we assume that the EW distribution is valid at $z = 5.7$ for 50 per cent IGM transmission, and that any change in the EW at higher z is due to the IGM only. Further, we assign the EWs completely randomly to our galaxies,

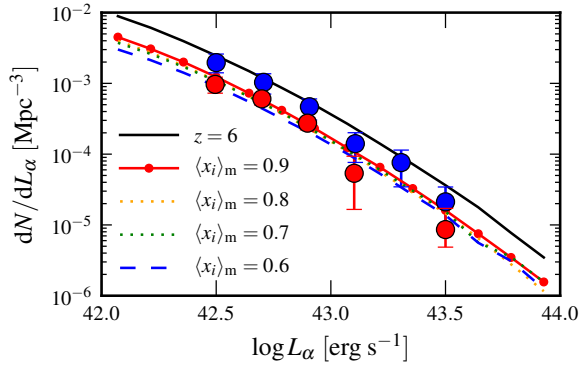


Figure 2. Ly α luminosity functions for the physical scenarios considered in this paper. The blue dots are observations by Ouchi et al at $z = 5.7$. Red dots are observations by Ouchi et al 2010 at $z = 6.5$. All the different simulated scenarios give luminosity functions that are indistinguishable from each other.

assuming that there is no correlation between Ly α luminosity and EW. This seems to be supported by observations, at least for objects with detectable EWs (Zheng et al. 2014; Hayes et al. 2014).

2.3 Physical scenarios

A large part of our focus in this paper is on the change in the Ly α emitter population between $z = 5.7$ and $z = 6.5$, since these are the highest redshifts where the HSC survey will obtain substantial samples. Previous observations have indicated that the Ly α luminosity function of Ly α emitters changes between these two redshifts (Ouchi et al. 2010; Kashikawa et al. 2011), but it is not clear whether this is due to an increasingly neutral IGM, a change in the intrinsic properties of Ly α emitters or a combination of the two.

For this paper, we will make the assumption that the luminosity function at $z = 6.5$ from Ouchi et al. (2010) holds true. We consider a number of different scenarios where there are varying degrees of change in the IGM ionized fraction and the intrinsic properties of the Ly α emitters. There are several possible mechanisms that could change the intrinsic properties of Ly α emitters, including changes in dust content and star formation rate (Verhamme, Schaerer & Maselli 2006; Laursen, Razoumov & Sommer-Larsen 2009; Guaita et al. 2011; Bish et al. 2013; Hayes et al. 2014). Here, we do not specify the mechanism responsible. Instead, we simply model intrinsic evolution by dimming/brightening all objects in our mock samples by some constant amount. Effectively, this means that we dim/brighten the objects both in Ly α and UV continuum luminosity so that their intrinsic EWs are unchanged. One could also imagine intrinsic processes that would alter Ly α and UV luminosities in different ways. However, this distinction is unlikely to have any major effects on the statistical observables we discuss here, i.e. clustering of galaxies.

We label our scenarios “ $\langle x_i \rangle_m = f$ ”, where f is the global mass-averaged ionized fraction of the Universe at $z = 6.5$. Our most extreme scenario is “ $\langle x_i \rangle_m = 0.6$ ” (i.e. the IGM is only 60 per cent ionized at $z = 6.5$). This is the ionized fraction we need in order to explain the change in the luminosity function without any intrinsic galaxy evolution between $z = 5.7$ and $z = 6.5$. Apart from this scenario, we also consider 70, 80 and 90 per cent ionization at $z = 6.5$. In these scenarios, the rest of the luminosity

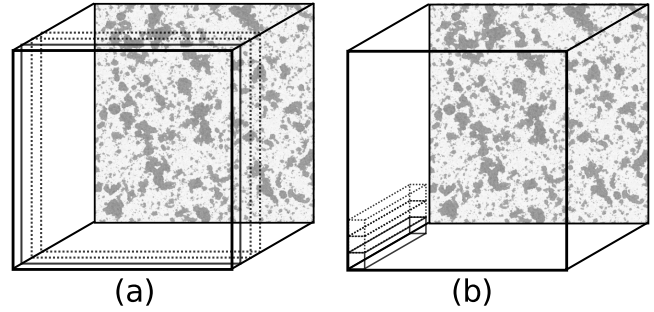


Figure 3. Schematic illustration of the sizes of our mock observations in relation to our full simulation volume. The left box (a) shows the HSC-like observations, where the width of the field is the full simulation volume, and the depth is $\Delta z \approx 0.1$. Here, we construct 10 samples along each coordinate axis. The right box (b) shows the JWST skewers, which have a field-of-view of 220 arcmin², and a depth of $\Delta z = 1$. We construct a total of 256 such skewers from our full volume.

evolution is due to intrinsic evolution (which we model by simply dimming all haloes by a constant factor).

Since we have only one reionization simulation, we have to construct these scenarios from simulation volumes that are nominally at different redshifts. For example, for the $\langle x_i \rangle_m = 0.6$ scenario, we use the C²-RAY output from $z = 7.5$ and increase all the halo masses so that the intrinsic luminosity function matches the one at $z = 5.7$. This is of course not entirely self-consistent, but since many studies have shown that the reionization topology is much more dependent on global ionized fraction than on redshift—at least if the relative contribution of high-mass and low-mass sources is similar—this method should still be reasonable (McQuinn et al. 2007a,b; Friedrich et al. 2011; Iliev et al. 2012; Taylor & Lidz 2014). To verify that the different redshifts do not have an appreciable impact on the intrinsic properties of our galaxies, we have calculated both the Ly α luminosity functions and the counts-in-cells variances (see Sec. 2.4) for the samples with the effects of the IGM removed. We found the differences between the samples to be negligible.

For each of the scenarios, we construct a number of mock HSC samples by first selecting all objects with $EW > 20 \text{ \AA}$, and then selecting the ones with the highest Ly α luminosities to give the same number density of Ly α emitters as the planned HSC survey (i.e. 5500 objects per 30 deg²). This gives similar effective luminosity cutoffs as those expected for the HSC survey, but we chose to specify exact number densities instead of exact cutoffs to make clustering comparisons easier. Since the redshift depth of the HSC survey is approximately one tenth of our simulation volume, we are able to construct ten mock observations for each coordinate axis for each scenario. Each such mock observation will have roughly half the area of the full HSC survey, so for some statistical predictions we combine two separate mock observations. Fig. 2 shows the Ly α luminosity functions of all these mock samples along with the observations of Ouchi et al. (2010) at $z = 5.7$ and $z = 6.5$. By design, they are indistinguishable when looking only at the luminosity functions. In Fig. 3 we show a schematic illustration of how the mock samples compare to our full simulation volume and to the mock samples for the JWST survey that we consider in section 3.4.

2.4 Clustering measurements

As can clearly be seen in Fig. 2, observations of luminosity functions alone are not useful for telling intrinsic galaxy evolution apart

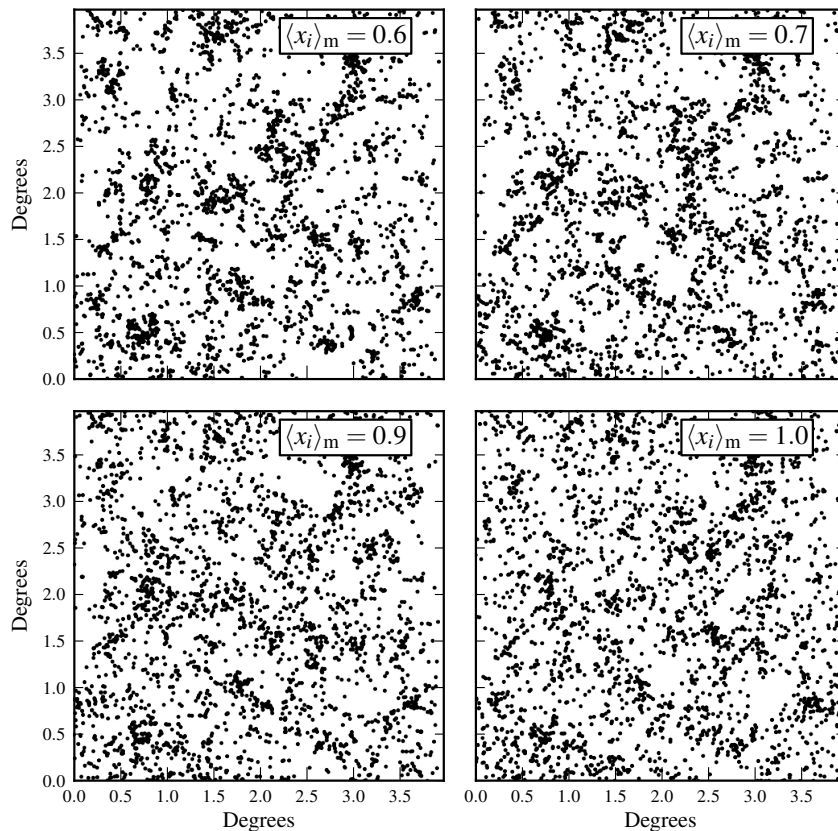


Figure 4. Observed Ly α emitters in a few sample mock HSC observations for some of our IGM evolution scenarios. The number density of objects in all panels is the same as expected for the HSC survey. However, the actual HSC field is roughly twice the area of our simulation. The additional clustering of objects in the less ionized scenarios is clearly visible.

from IGM evolution. However, by looking at the spatial clustering of Ly α emitters, it may be possible to separate the two effects. When doing this, it is important to distinguish the clustering that comes from the topology of the ionized bubbles (which is what we are interested in here) from other sources of clustering.

In addition to the intrinsic clustering of galaxies due to density fluctuations in the Universe, a partially neutral IGM will affect the clustering of Ly α emitters in two ways (McQuinn et al. 2007a; Mesinger & Furlanetto 2008; Iliev et al. 2008). First, if one considers two observed samples with the same luminosity cutoff but different IGM ionized fractions, the sample with the most neutral IGM will have a higher clustering of sources. This is mainly because only the most massive sources will be seen through the more neutral IGM, and these are also the ones that are found in the densest regions.

Second, if one considers two samples again with different IGM ionized fraction, but with the same number of observed sources (implying different luminosity cutoffs), then the clustering of sources will also be increased since Ly α emitters are easier to observe if they are located deep inside an ionized region. High-luminosity Ly α emitters that happen to lie at the edge of an ionized region may be obscured, while slightly lower-luminosity sources that are in the middle of an ionized region may be observ-

able. However, since the ionized regions are not located at random, but are localized around the largest clusters of galaxies, this effect is fairly weak and requires large samples to observe.

The first of these two effects is simply due to the decrease in number density, and cannot be used to separate intrinsic galaxy evolution from IGM evolution. The second one, on the other hand, is a signature of a partially ionized IGM. Therefore, we consider only samples with a fixed number density. A visual illustration of the IGM-induced clustering for a fixed sample size is shown in Fig. 4, where we show the detected Ly α emitters in four of our scenarios for the mock HSC survey.

There are several ways to quantify the spatial clustering of galaxies. One of the most common methods is the two-point correlation function, $w(\theta)$, which is the excess probability of finding two galaxies at a separation θ , compared to a uniform random distribution. The two-point correlation function contains a lot of information since it measures the clustering over a range of scales. However, comparing two different correlation functions is usually done by fitting a parameterized functional shape, which requires implicit assumptions about the statistics of the objects in the sample. Furthermore, the two-point correlation function is awkward to calculate for fields with complicated shapes.

Here, we consider instead a related statistic called *counts-in-*

cells. The counts-in-cells method works by simply dividing the observed field into a number of cells of equal size and counting the number of galaxies n_i that fall into each cell i . Typically, one then calculates the variance of the counts:

$$\sigma_{\text{cic}}^2 = \frac{1}{N} \sum_{i=0}^N (n_i - \langle n \rangle)^2 \quad (4)$$

where N is the total number of cells. The counts-in-cells variance gives us a single, easy to calculate, number that measures the clustering without any assumptions of the statistics of the objects—higher variance means more clustered objects. In fact, σ_{cic}^2 can be shown to be proportional to the integral of the two-point correlation function (see e.g. Adelberger et al. 1998 and Mesinger & Furlanetto 2008 for more details). The two major drawbacks of the method are that the results depend on the choice of the cell size, and that it contains no information about the clustering on different spatial scales (as opposed to the correlation function).

2.5 Bubble mapping

The counts-in-cells method discussed above requires only that we know the positions of Ly α emitters. However, if we know also the EW of the galaxies in our sample, we can use this to learn more about the IGM. Since the UV luminosity is not affected by neutral hydrogen in the IGM¹, the EW—i.e. the ratio between the Ly α and the UV continuum luminosity—will be a measure of T_α , the fraction of Ly α flux that is transmitted through the IGM.

For an individual galaxy, calculating T_α from the EW is fairly meaningless, since the random scatter is very large (cf. Fig. 1). However, with a sample containing thousands of galaxies, it becomes possible to look for trends in the observed EW in different regions on the sky. We would expect the EW to be higher on average in regions where the IGM is highly ionized. By studying the mean EW in different regions, it may be possible to reconstruct the ionization structure of the IGM and measure the locations and sizes of the largest ionized regions (or “bubbles”). Such “bubble mapping” may give valuable insights into the topology of reionization.

3 RESULTS

The HSC survey will attempt to measure both the Ly α and UV continuum luminosities of Ly α emitters at $z = 5.7$ and $z = 6.5$. In total, the survey is expected to detect approximately 5500 objects at $z = 6.5$ using the narrow-band selection technique (M. Ouchi 2013, private communication). In this section, we give predictions for how accurately this survey will be able to constrain reionization. We begin by looking at the case where only Ly α luminosities are available. In section 3.2 we consider the case where we also know the UV luminosities. In section 3.4 we investigate what can be done with a spectroscopic survey carried out using the JWST, where we would know the redshifts of objects in a field with a small area, but a large extent along the line-of-sight.

¹ It is true that the part of the continuum on the blue side of the Ly α line will be subject to IGM absorption, but at redshifts $z \gtrsim 6$, this absorption is essentially a complete Gunn-Peterson trough, and can be corrected for. The presence of a Ly α damping wing will introduce a slight uncertainty to the correction, but for a broad-band measurement, this uncertainty will be small.

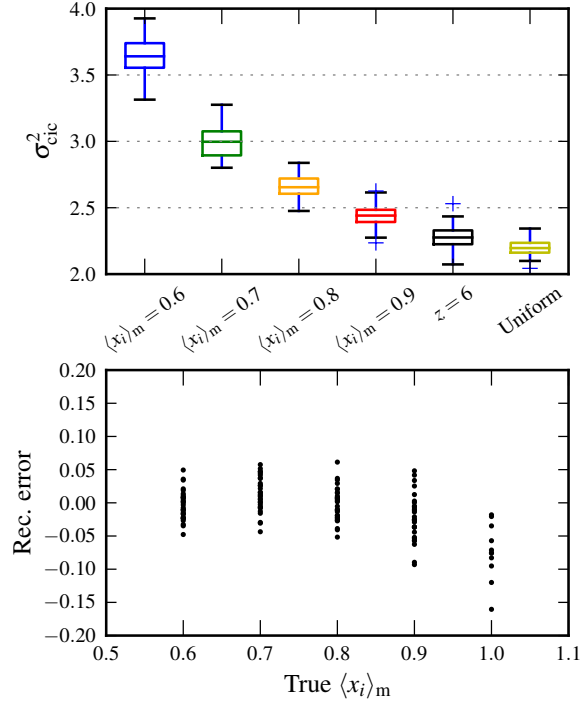


Figure 5. The clustering of Ly α emitters caused by a neutral IGM. *Upper panel:* Counts-in-cells variances for our four scenarios and for the case of a uniform random distribution. The horizontal lines show the median of 30 different slices through the box. The boxes show the quartiles, the whiskers show the range of the data and the + signs show the outliers. *Lower panel:* The difference between the true $\langle x_i \rangle_m$ and the reconstructed value obtained by fitting a second-degree polynomial to the σ_{cic}^2 values as a function of $\langle x_i \rangle_m$.

3.1 HSC observations with Ly α luminosities only

If the only available information about a galaxy is its Ly α luminosity, it is impossible to say anything about the Ly α transmission through the IGM for that particular galaxy. However, we can still say something about the ionization state of the IGM through clustering analysis, as discussed in section 2.4.

In the upper panel of Fig. 5, we show the counts-in-cells variance σ_{cic}^2 for our four scenarios, using 50×50 cells, i.e. a cell size of 4.8×4.8 arcmin. This choice of cell size is somewhat arbitrary, but we have found that the results are not very sensitive to the exact cell size. Since our simulation area is half the size of the HSC field, we construct a mock measurement by combining two different slices of the volume. We do this for 30 different pairs of slices (we take 10 slices from the simulation volume along each coordinate axis, each with a depth of $\Delta z \approx 0.1$) to get an idea for the sample- and cosmic variance. The horizontal lines in Fig. 5 show the medians of these 30 values of σ_{cic}^2 .

The actual values of σ_{cic}^2 are not important to us here. Instead, we are interested in the difference between the clustering at $z = 6$ —where we assume that the IGM is almost entirely ionized (e.g. Songaila 2004)—and $z = 6.5$. Comparing σ_{cic}^2 for samples with the same number of objects at these two redshifts, we may ask ourselves whether the change in clustering is consistent with a fully ionized IGM at $z = 6.5$ or not.

The variation in the measured σ_{cic}^2 comes both from Poisso-

nian sample variance and from fluctuations in the underlying density field and the ionization fraction (cosmic variance). To better see the contribution of these effects, we performed the same calculations of σ_{cic}^2 as discussed above, but for uniformly distributed samples with the same number density as our mock observations (labelled “Uniform” in Fig. 5).

The variation in σ_{cic}^2 for the uniform samples is due only to sample variance. Comparing to the mock observations with a fully ionized IGM, we see that the variation is very similar in magnitude, indicating that the cosmic variance is negligible for such large samples, at least for the scenarios with higher ionization fraction². For the $\langle x_i \rangle_{\text{m}} = 0.6$ scenario, the variation in σ_{cic}^2 is roughly twice as large, due to the ionization fraction fluctuations.

Since the cosmic variance is negligible for a highly ionized IGM, any detection of a clustering signal that is higher than the $z = 5.7$ clustering by more than the sample variance would be a strong indication of a significantly neutral IGM. Judging by Fig. 5, a sample with the size of the HSC survey can be used to robustly rule out a global ionization fraction of $\langle x_i \rangle_{\text{m}} \lesssim 0.8$ at $z = 6.5$. However, a neutral fraction as small as 10 per cent would be difficult to reliably detect with this method.

We also try to use reconstruct the global ionization fraction from the measured σ_{cic}^2 values. To do this, we make a simple second-degree polynomial fit to the values in the upper panel of Fig. 5 as a function of $\langle x_i \rangle_{\text{m}}$ and invert this relation to give $\langle x_i \rangle_{\text{m}}$ as a function of σ_{cic}^2 . The points in lower panel of Fig. 5 show the error in the reconstructed ionized fraction for each of our mock samples. The polynomial fit is very simple model, and seems to work somewhat unsatisfactorily at high $\langle x_i \rangle_{\text{m}}$; however, it serves the purpose of illustrating the general uncertainty in the reconstructed ionized fraction. We see that in general, we can recover the global ionized fraction with an uncertainty Δx_i that is typically $\lesssim 0.1$.

Of course, such a reconstruction assumes that our model for the Ly α emitters and the IGM is correct. There are a number of aspects of the model that can potentially affect the results. First, the model for the intrinsic Ly α line shape can make the observed luminosity more or less dependent on the surrounding IGM, as discussed in more detail e.g. by Dijkstra, Mesinger & Wyithe (2011) and Jensen et al. (2013). In general, the larger the part of the Ly α line that is offset from the line center, the less sensitive the transmission will be to the damping wing from the IGM, and the smaller the clustering due to neutral IGM will be. The line model we use here has no emission directly at the line center, and is thus relatively insensitive to the IGM. The intrinsic random scatter that we include in the Ly α luminosity will also affect the clustering: the more random the luminosities, the smaller the relative effect of the IGM on the object selection will be. The random scatter we include effectively includes both the randomness in the amount of Ly α that is produced in galaxies and the amount that escapes in different directions. These quantities are not well known, but looking at Fig. 2 it seems clear that including a larger random scatter than the one we use here would make the Ly α luminosity function too flat to be compatible with observations (since more random scatter makes the luminosity less dependent on halo mass, which makes the luminosity function flatter). On the other hand, it may be possible to fit the luminosity function with a more complicated distribution of Ly α luminosities, for example a bimodal distribution (i.e. a “duty cycle” scenario).

² Note that the actual values of σ_{cic}^2 are lower since these data points are uniformly random, with no intrinsic galaxy clustering.

The simulation of the IGM can also affects the results. The simulation we used here only distinguishes between two types of sources of ionizing radiation (big and small). Changing the source model would change the IGM-induced clustering to some extent. For example, we could imagine an extreme scenario where all dark matter haloes are hosts to sources of equal ionizing flux. In this case, the IGM-induced clustering would be relatively small, since all galaxies would ionize the region around them to the same extent. On the other extreme, if there were only a few very bright ionizing sources, the clustering signal would be stronger since the observability of a Ly α emitter would depend strongly on whether it was located inside one of the few large H II regions produced by a massive source. However, in most realistic models, each H II region is produced by tens or hundreds of sources, and so for a fixed global ionization fraction, the results will not be strongly dependent on the relative efficiencies of different sources.

In addition to the model dependence, Fig. 5 shows that cosmic- and sample variance add a significant degree of uncertainty. However, if the test is performed as a simple null hypothesis test (i.e. asking the question “is the IGM at $z = 6.5$ consistent with fully ionized IGM or not?”), model dependence is no longer a big issue.

3.2 HSC observations with Ly α and UV luminosities

We now consider the much more optimistic case where we have measurements of not only the Ly α luminosity, but also the Ly α EW (which requires detections in the UV continuum as well). This is unlikely to be true for all galaxies after the initial HSC narrow-band survey, but it may be possible to perform follow-up observations to detect the UV continuum level in a larger number of galaxies. For this section, we assume—optimistically—that we know the EW for all the galaxies in the HSC sample. As such, our results in this section represent an upper limit on the statistics that will be possible using EWs.

Observations have shown no correlation between Ly α luminosity and EW (Zheng et al. 2014), and we would expect that in a fully ionized IGM, the EW of an object would be independent of its position on the sky. However, since the EW will be attenuated by H I absorption, a patchy ionization structure of the IGM would introduce a position dependence in the EW distribution. A possible way of looking for signs of reionization would therefore be to test whether the observed EW distribution shows any signs of spatial clustering.

One could think of many ways of performing such a test, but one test that we have found to perform particularly well is to measure the correlation between the number of neighbours of a galaxy and the mean EW of these neighbours. More precisely, we conduct this test as follows:

- (i) For each galaxy:
 - Locate all galaxies within some distance d on the sky-plane.
 - Count the number of such neighbour galaxies and calculate their mean EW.
- (ii) Measure the Pearson correlation coefficient r between the number of neighbours and the mean neighbour EW.
- (iii) Take all measured EWs and randomly reassign them to another galaxy, to create a new sample with no correlation between EW and position on the sky. Repeat steps (i) and (ii) for the shuffled sample.

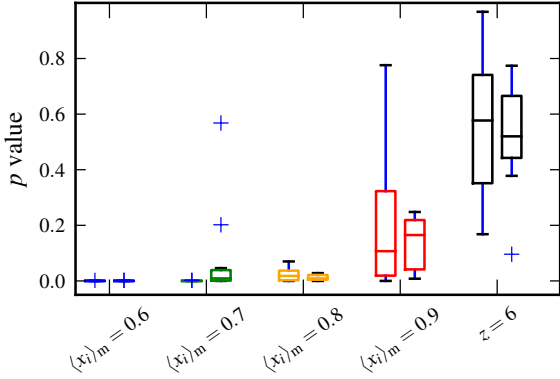


Figure 6. Results from measuring the correlation between the number of neighbour galaxies and the mean EW of the neighbours (see the text for details). The p values indicate the likelihood of obtaining the observed correlation coefficient if IGM is completely ionized at $z = 6.5$. For each scenario, the boxes to the left are for the narrow EW model, while those to the right are for the fiducial EW model.

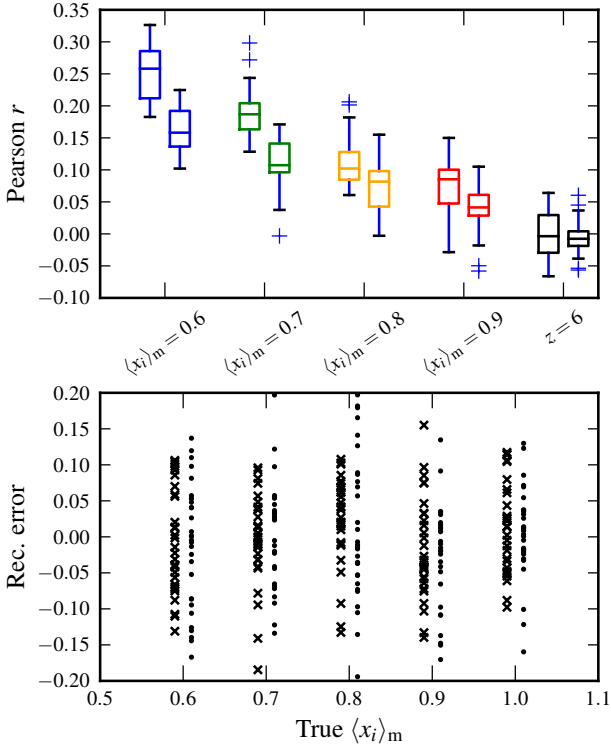


Figure 7. *Upper panel:* Same as Fig. 6, but now showing the actual measured Pearson correlation coefficients between the number of neighbours and the mean neighbour EW for our different scenarios. Again, for each scenario, the boxes to the left are for the narrow EW model, while those to the right are for the fiducial EW model. *Lower panel:* The difference between the true $\langle x_i \rangle_m$ and the value reconstructed by fitting a straight line to the correlation coefficients in the top panel. The crosses are for the narrow EW model, while the points are for the fiducial model.

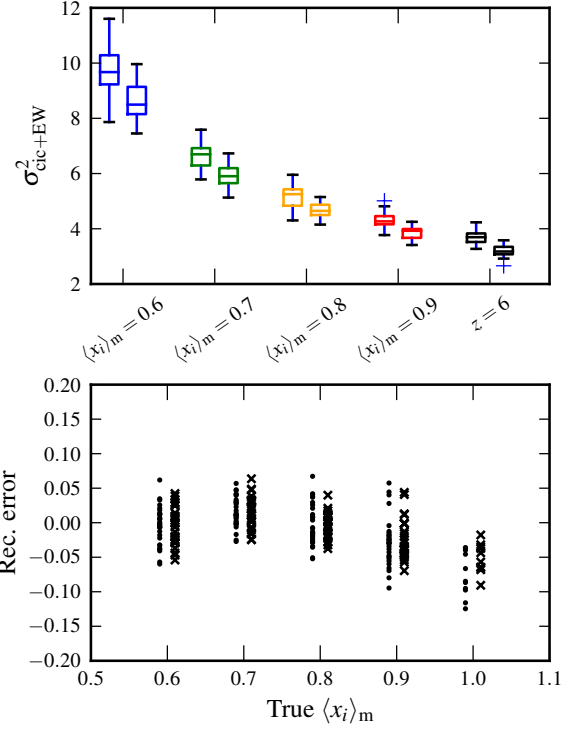


Figure 8. Same as Fig. 5, but for the counts-in-cells combined with the smoothed EW.

- (iv) Repeat step (iii) many times to create a distribution of r values with no correlation.

Using this procedure we can calculate a p value for the null hypothesis—that the IGM is fully ionized—by counting the fraction of shuffled samples that give a higher value of r than the original sample. We have tested our method on the publicly available sample of Ly α emitters of Nilsson et al. (2009). Running our test on their $z = 2$ objects (where we expect no clustering from the IGM) for a number of different values of d , we find no signs of correlation between the number of neighbours and the neighbour-smoothed EWs. While this sample is much smaller than our simulated volume (187 objects in a 35×34 arcmin region) it is still encouraging to see that there does not seem to be any signs of intrinsic correlation in lower-redshift data.

Our results for this test on our simulated data for both of our EW models (see section. 2.2), using a neighbour distance $d = 20$ cMpc, are shown in Fig. 6. For each of our scenarios we analyze the same 30 independent mock observations as in section 3.1, each with the same size as the HSC survey. We use 500 shuffled samples to calculate the distribution of correlation coefficients for the case of the null hypothesis.

As Fig. 6 shows, with a sample of this size, this method can robustly rule out a global ionized fraction lower than 80 per cent at high confidence level, at least for the narrow EW model. Already at 90 per cent ionization, it may be possible to infer some neutral IGM, albeit with a lower significance.

Besides making use of more information (since we have both UV and Ly α luminosities), this test has the advantage of being “self-contained”, since we can directly compare to a random EW

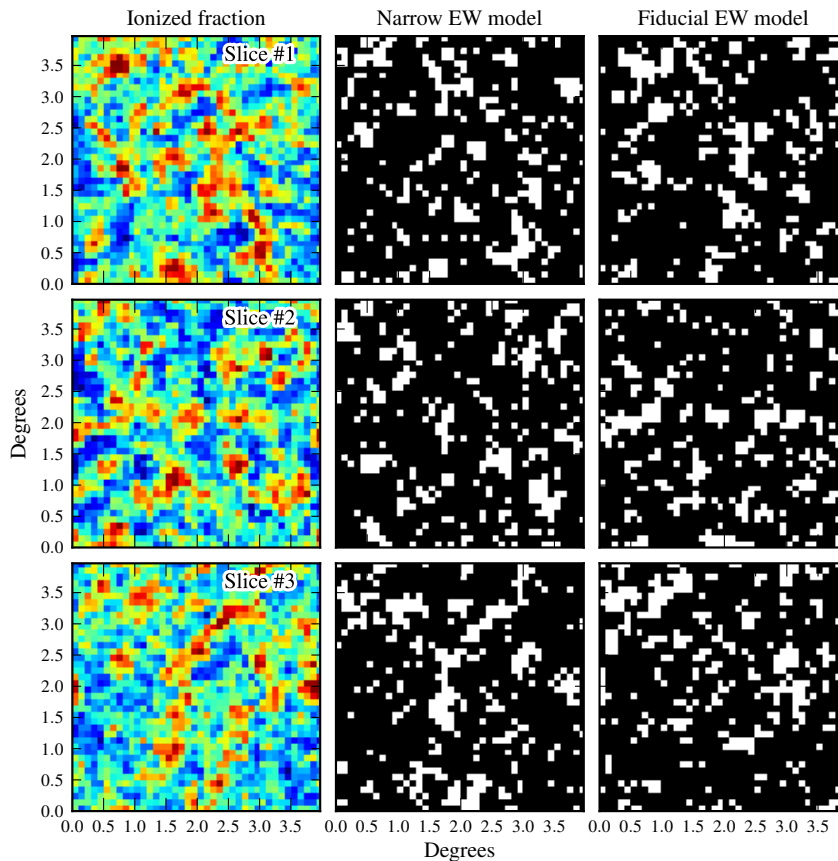


Figure 9. Bubble mapping using smoothed EWs for the $\langle x_i \rangle_m = 0.6$ scenario for three sample slices through the simulation volume. The left column shows the true ionized fraction, with blue indicating completely neutral, and red completely ionized. The middle and right columns show the smoothed and gridded Ly α EWs for our two EW models. To better see the ionized regions, we show cells with EWs above the 80th percentile as white, and all other cells as black.

distribution. While the counts-in-cells test relies on comparing to observations at lower redshifts, the neighbours–EW test directly gives us a likelihood of the IGM being completely ionized at $z = 6.5$.

In Fig. 7 we show the values of the Pearson correlation coefficients, similarly to the counts-in-cells variances in Fig. 5. We also show the errors in reconstructed ionization fractions obtained by fitting a linear relation between correlation coefficient and $\langle x_i \rangle_m$, similarly to what we did in the previous section. From this figure, it would seem that for determining the global ionization fraction, the neighbour–EW method performs roughly as well as simple counts-in-cells, but seems slightly more sensitive to small amounts of neutral IGM.

It is also possible to combine the information from the EW distribution with the count-in-cells test from the previous section. To do this, we count the number of galaxies in each cell, as before, and multiply that number with the normalised average neighbour-smoothed equivalent width in that same cell. We then calculate the variance $\sigma_{\text{ci+EW}}^2$ of this new quantity. The results of this test are shown in Fig. 8. From this figure, we see that including the EWs improves the counts-in-cells measurement slightly, to the point where the global ionization fraction can generally be recovered with an error of $\Delta x_i \lesssim 0.05$.

Aside from the observational difficulty involved in obtaining reliable EWs for all the narrow-band selected objects, this method has the drawback of being dependent on the intrinsic EW distribution assumed, as is clear from Fig. 7. The wider the distribution is, the more the variation of EWs will be due to random scatter rather than varying IGM transmission. If this method was to be used to constrain the global ionized fraction for real data, one would likely want to calibrate it to better observations of the EW distribution at $z = 5.7$.

3.3 HSC bubble mapping

A test such as the neighbours–EW correlation test described in the previous section can tell us whether there is some spatial structure to the EW distribution, but it will not provide any information about the sizes, shapes and locations of ionized regions. However, if the IGM should turn out to be significantly neutral at $z = 6.5$, so that there are in fact distinct ionized bubbles in which most galaxies reside, it may be possible to extract a crude “image” of the ionization state of the IGM by comparing the observed EWs at different positions on the sky.

In Fig. 9, we have taken the objects in the $\langle x_i \rangle_m = 0.6$ scenario and smoothed the EWs by setting each EW to be the mean

of all the EWs within $d < 20$ cMpc. We have then divided the field into a grid of 40×40 cells and calculated the mean smoothed EW in each cell³. We compare this to the IGM ionized fraction in a skewer extending 50 cMpc towards the observer (left column; down-sampled to the same cell size as the EWs). To better see the results we show cells with an EW below the 80th percentile as black, and everything else as white. This makes it easier to locate the regions with particularly high EWs. We show the results for three independent slices through our simulation volume for both EW models.

Although there is a large amount of noise in the “images”, the largest ionized structures can clearly be identified for the narrow EW model (middle column). Note for example the elongated ionized structure extending from the middle to the top-right corner of slice 3, and the ‘J’-shaped structure in the lower-right corner of slice 1, both of which are clearly visible in the panels on the right. However, for the fiducial EW model (right column), the results are less optimistic. A few of the largest structures are still visible, but they are difficult to distinguish from the random noise.

In Fig. 10 we show the mean EW in each cell in the bottom panel (slice 3) of Fig. 9 and the mean ionized fraction in front of the slice. This figure shows that while there is a large random scatter, there is a clear correlation between the EW and the local ionization state of the IGM. The correlation is significantly stronger for the narrow EW model than for the fiducial model, however, since there is more random scatter in the EWs for this model.

3.4 JWST observations

Next, we consider a hypothetical small-field, deep spectroscopic survey, as might be carried out using the JWST with the NIRSpec instrument. We assume a survey consisting of 25 NIRSpec fields, for a total area of 225 arcmin² and a redshift range of $6 < z < 7$. To select drop-out targets for NIRSpec, one first needs a photometric survey reaching $m_{AB} \approx 28.5$ mag. Reaching this limit with $S/N \approx 5$ in the F070W, F090W and F115W filters, takes ≈ 3 h per sub-field, which implies 75 h of NIRCам imaging in total. To improve the dropout selection, auxiliary imaging at shorter optical wavelengths would also be very valuable, and HSC seems to be the ideal instrument for this—a single HSC field exposed for ≈ 14 h would for instance be sufficient to add $m_{AB} \lesssim 28.5$ mag data in the g -band ($0.45 \mu\text{m}$). Based on the luminosity functions of dropout selected galaxies (Bouwens et al. 2007, 2011) we estimate that there should be ≈ 1650 targets for spectroscopic follow-up in our survey, between $6 < z < 7$. Using the NIRSpec exposure time calculator (v P1.6), and assuming an exposure time of 3 hours per sub-field ($3 \text{ arcmin} \times 3 \text{ arcmin}$), we find that it should be possible to measure the Ly α EW with acceptable S/N for objects with $\text{EW} > 40 \text{ \AA}$, and the redshift down to an uncertainty of $\Delta z \lesssim 0.1$ for objects $\text{EW} > 10 \text{ \AA}$.

While the number densities that we obtain even for such an ambitious survey are much lower than those expected for the HSC survey, there are other aspects that make a survey such as this interesting to consider. Since we are measuring the spectra of objects, we can obtain their line-of-sight positions, and we are thus probing the IGM in a skewer along the redshift axis, rather than in a plane

³ The neighbour-smoothing is similar in nature to a convolution operation, and improves the results compared to only performing the gridding, since it smooths the EWs based on all the neighbours, not just those that happen to be in the same grid cell.

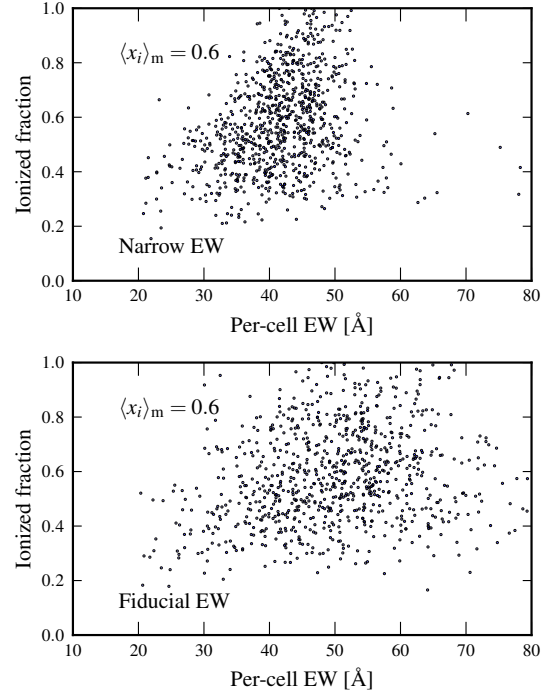


Figure 10. Correlation between the local ionized fraction and the neighbour-smoothed EW of each cell in the third row (slice 3) in Fig. 9.

on the sky (see Fig. 3). Since the area on the sky of such a skewer is small compared to typical sizes of ionized regions, this type of measurement is essentially one-dimensional along the line-of-sight. This makes such measurements fundamentally different from those discussed earlier in the paper, since the survey will probe galaxies across a large range of epochs (the redshift range of our hypothetical JWST survey is $\Delta z = 1$, which is 10 times that of the HSC survey).

Previous similar surveys have focused mainly on the evolution of the fraction of dropout selected galaxies that show Ly α emission. There is now strong observational support that this fraction drops sharply between redshifts 6 and 7 (Pentericci et al. 2011; Stark, Ellis & Ouchi 2011; Schenker et al. 2012; Pentericci et al. 2014; Tilvi et al. 2014). This drop could be explained by neutral IGM, intrinsic galaxy evolution or some combination between the two. Analogous to the first part of the paper, we would like to investigate whether a larger survey may be able to break this degeneracy by looking at higher-order statistics.

To account for the change in number density of objects and IGM transmission, we construct our mock JWST observations by combining our different scenarios from section 2.3. We construct a new data volume by assuming that the IGM is 30 per cent ionized at the high-redshift end of the observations (which we put at $z = 7$). This is the ionized fraction required to reproduce the results of Schenker et al. (2012) and Pentericci et al. (2014), if the evolution in the EW distribution is due to neutral IGM only. We make this new data volume by taking slices of data from the different scenarios and putting together a new volume that goes from $z = 6$, where the ionization fraction is 95 per cent, up to $z = 7$, where the ionization is 30 per cent. For the rest of this section, we will refer to this scenario as “Simulated IGM”. For comparison, we

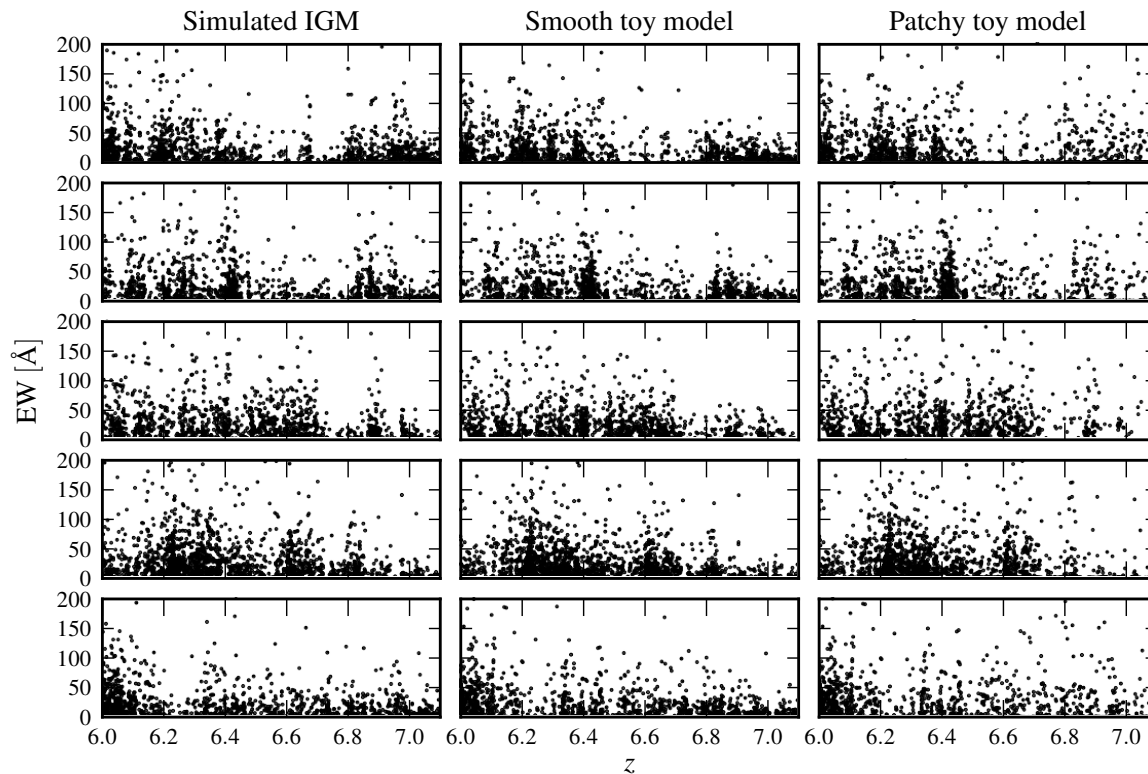


Figure 11. Redshifts and EWs of the objects in a few example skewers for our three evolution scenarios. Each row shows one example mock observation. The values shown in these plots are the intrinsic values of the drop-out selected galaxies, not the values that would be measurable from spectroscopy.

also construct a similar volume where the IGM is 95 per cent ionized all the way up to $z = 7$. Then, we divide both of these volumes into skewers, and select the most massive objects to give the correct number density of observed drop-out galaxies (approximately 1650 objects per skewer). In total, we construct 256 different skewers, each representing a mock JWST observation.

Using the volume with a fixed, 95 per cent, ionization state we also construct two scenarios with intrinsic EW evolution. In the first of these scenarios, which we will refer to as the “Smooth toy model”, the EWs of galaxies at a redshift z are dimmed by a factor $\epsilon_s(z)$. This is equivalent to a distribution of transmitted fractions of Ly α photons that is just a delta function at a given redshift: $p(T_\alpha) = \delta(T_\alpha - \epsilon_s)$. We tune $\epsilon_s(z)$ to give the same fraction of galaxies with $EW > 25 \text{ \AA}$ as the scenario with neutral IGM at all z .

In the second scenario, termed “Patchy toy model”, a fraction $\epsilon_p(z)$ of galaxies at each redshift z are turned off completely, while the rest are left unchanged. This is equivalent to a distribution of T_α that follows a bimodal function with one peak at $T_\alpha=0$ and one peak at $T_\alpha=1$. This model was first used by Treu et al. (2012) as a simplified view of a partially ionized IGM. However, in contrast to the simulations, there is no spatial correlation in the patchiness in this model—a galaxy with $T_\alpha = 0$ may lie right next to one with $T_\alpha=1$. Figure 12 shows the fraction of Ly α emitters as a function of redshift for our three evolution scenarios (note that these are tuned to be very similar).

Clearly, as Fig. 12 shows, different evolution scenarios can give very similar Ly α emitter fractions. A different approach to

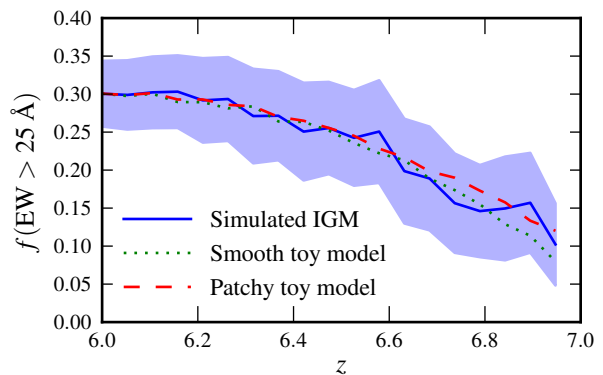


Figure 12. Fraction of galaxies with $EW > 25 \text{ \AA}$ as a function of redshift for our three different evolution scenarios. The fractions show are the total numbers for the entire simulation volume, i.e. 256 different mock JWST observations for each scenario. The shaded blue area shows the 1σ field-to-field variation for the Simulated IGM scenario (omitted from the other scenarios for visual clarity).

separating scenarios is to compare the distribution of EWs at two different redshifts. The difference in EW distribution contains more information than simply the fraction of objects that fall above some EW limit. Very recently, Pentericci et al. (2014) claimed that their observations of Ly α emitters strongly favoured a patchy evolution over a smooth one between redshifts 6 and 7, and similar results

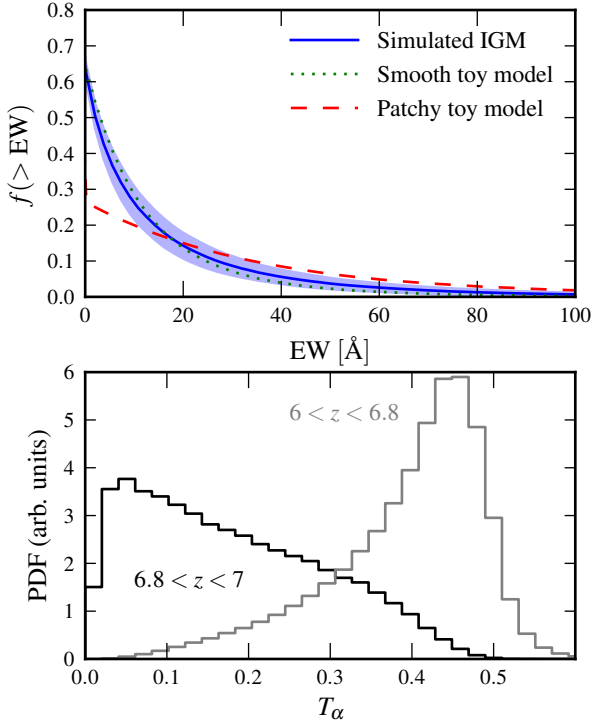


Figure 13. *Upper panel:* Cumulative EW distributions for all mock JWST observations for our three different evolution scenarios at $z > 6.8$. The shaded blue regions shows the 1σ field-to-field variation for the Simulated IGM scenario. *Lower panel:* Probability density distributions (PDFs) of the IGM transmission fraction T_α for the Simulated IGM scenario for high and low redshifts.

were found by Tilvi et al. (2014) at $z \sim 8$. This was interpreted as supporting a patchy reionization as the explanation for the drop in Ly α emitter fraction.

However, as Fig. 13 shows, our simulations (the Simulated IGM scenario) are much more similar to the smooth evolution model than the patchy model. The top panel of this figure shows the cumulative EW distribution for the high-redshift part of all our JWST-like skewers. We see that the simulations produce an EW distribution that is almost indistinguishable from the smooth evolution scenario. Pentericci et al. (2014) found a few objects at $z \sim 7$ with relatively high EW, but a significant shortage of intermediate-EW objects. The patchy model gives exactly such a distribution, because it is equivalent to a bimodal T_α distribution. However, as the bottom panel of Fig. 13 shows, a neutral IGM does not produce a bimodal distribution of T_α in our simulations.

Therefore, it would seem that the results of Pentericci et al. (2014) actually argue *against* patchy reionization, or at least the type of patchy reionization produced by neutral IGM in our simulations. A future survey such as the one described in this section would of course provide much better measurements of the EW distribution of high-redshift Ly α emitters, but as Fig. 13 shows, the EW distribution is not a very sensitive probe of different reionization scenarios, and is in fact not very useful for distinguishing between evolution due to neutral IGM and smooth intrinsic evolution.

As we discussed in the first part of the paper, a distinguishing feature of reionization is that T_α for a given galaxy depends

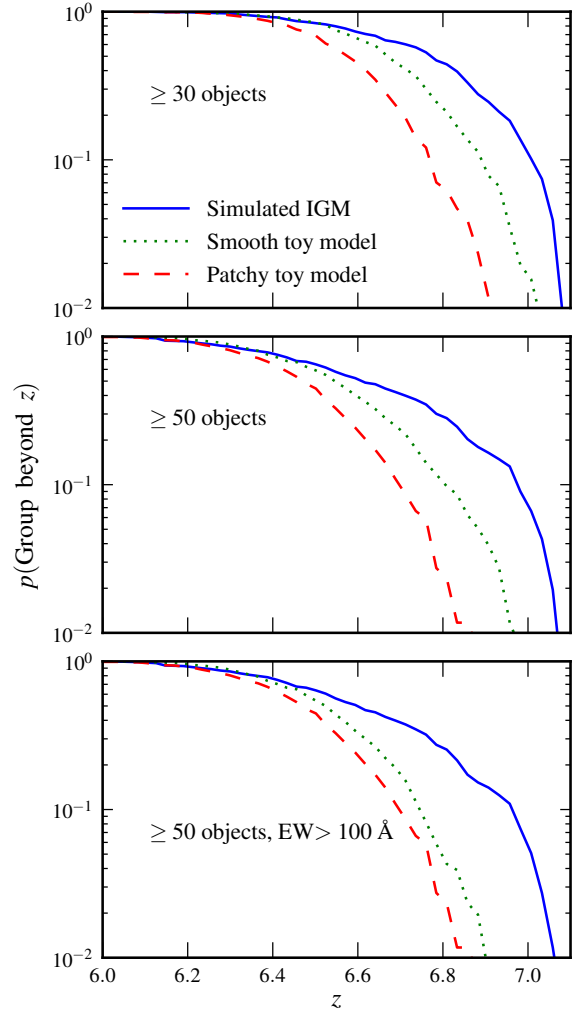


Figure 14. Probability of finding a group of more than 30 (upper panel) and 50 (middle panel) Ly α emitters beyond a given redshift for the type of JWST-like survey considered here. The lower panel shows the same as the middle panel, but now requiring that each group contain at least one object with $EW > 100 \text{ \AA}$.

to some degree on the location of that galaxy. For the mock HSC observations, we quantified this using the counts-in-cells method and the neighbours-EW correlation. Unfortunately, these types of methods are much less effective for samples that come from a wide range of redshifts. For example, in all our mock JWST observations there is a strong correlation between number of neighbour galaxies and the EW, simply because there is a higher density of galaxies at lower redshift, and the EWs of these galaxies are less attenuated, regardless of the evolution scenario.

Looking at Fig. 11, it is also clear that the Simulated IGM and the Smooth toy model scenarios are not hugely different from each other, and that the field-to-field variation is rather large. However, there does seem to be a tendency for high-redshift galaxies to be slightly more clustered in the Simulated IGM scenario, which is what one would expect if the skewer happens to cross a large ionized region. We quantify this by identifying groups of galaxies using a one-dimensional friends-of-friends algorithm along the line-of-sight. We assume that our spectroscopic survey can detect the redshifts of objects with $EW > 10 \text{ \AA}$ with an accuracy of

$\Delta z = 0.1$, and identify friends-of-friends groups using a linking-length of 2 cMpc. We do this for all our 256 skewers for each evolution scenario.

In Fig. 14 we show the results of this analysis. We show the probability that a single JWST observation will contain a group of galaxies of a certain size beyond a given redshift. We see here that the three evolution scenarios are fairly similar up to $z \approx 6.5$. However, beyond this redshift, the Simulated IGM scenario contains significantly more groups. This difference is a direct consequence of the spatial correlation of T_α . Judging by Fig. 14, finding a group of at least 50 Ly α emitters at $z > 6.8$ would be a strong indication of reionization, and would be unlikely for any of the other evolution scenarios. This would only happen if the skewer happened to cross a particularly large ionized region, which is not extremely likely if the survey field is chosen at random. However, it may be possible to target fields with bright quasars, which are likely to be located in very biased regions.

We can separate the scenarios even further by requiring that the groups of galaxies contain at least one object with an EW above some threshold value. We show the results for the threshold value of 100 Å in the bottom panel of Fig. 14. We see from this figure that the chances of detecting a group of at least 50 Ly α emitters beyond $z = 6.8$, of which at least one has an EW > 100 Å, is approximately 30 per cent if the evolution in EW distribution is due to neutral IGM only. This is three times as likely as the other two evolution scenarios. At $z > 6.9$, there is still a 10 per cent chance of finding such a group in the Simulated IGM scenario, whereas the probability is negligible for the other two scenarios.

In summary, when it comes to using JWST observations of Ly α emitters to directly constrain the ionized fraction of the IGM, our results look somewhat less promising than for the HSC. Even a very ambitious survey like the one considered here will only be able to detect a small fraction of the objects that are detectable with the HSC. Furthermore, since the observations span a large redshift interval, any effects of the IGM will be mixed together with intrinsic evolution. Nevertheless, with a bit of luck there is a possibility that a JWST survey will detect a large group of galaxies at very high redshift. This would be a strong indication of reionization, but not a firm proof on its own, since other evolution scenarios also have a non-negligible probability of producing false positives.

Even without such luck, a survey like this will still be useful for studying reionization. What we have considered here is only the observability of the statistical effects of a partially neutral IGM on a population of Ly α emitters, but a deep spectroscopic survey will produce a great deal of information about the physical properties of the galaxies that are likely to have been the sources of reionization. Knowing more about the ages, sizes and star formation rates of these objects will be an important piece in the EoR puzzle, and deep JWST/NIRSpec observations of the type proposed here may even be able to constrain the escape fraction of ionizing radiation from some of the brightest EoR galaxies (Zackrisson, Inoue & Jensen 2013).

4 SUMMARY AND DISCUSSION

Using a large-scale simulation of the IGM during reionization combined with Ly α radiative transfer simulations, we have explored the new types of statistical measurements of the ionization state of the IGM at $z \gtrsim 6$ that will become possible with the next generation of large Ly α emitter surveys. Surveys with instruments such as the HSC and JWST/NIRSpec will provide improved measurements of

many important properties of high-redshift Ly α emitters, such as their luminosity function, their typical sizes, ages, star formation rates etc. However, such measurements only give indirect information about the history of reionization. In this paper, we have instead focused mainly on methods to break the degeneracy between neutral IGM and intrinsic galaxy evolution.

Clustering measurements such as counts-in-cells provide a way of separating the effects of a neutral IGM from intrinsic galaxy evolution. While changes in star formation rate, escape fraction or dust content may all help explain the apparent decrease of Ly α emitters between $z = 6$ and $z = 6.5$, it is unlikely that any of these processes would produce a clustering signal that could be confused with a neutral IGM.

We find that, if only Ly α luminosities are available, the Subaru Hyper-Suprime Cam (HSC) survey should be able to distinguish an IGM that is $\gtrsim 20$ per cent neutral from one that is completely ionized at $z = 6.5$ by measuring the clustering of Ly α emitters, for example using the counts-in-cells method.

If the UV continuum luminosities can also be measured, several new possibilities open up. We have shown that by measuring the correlation between the mean EW of all the close neighbours of a galaxy and the number of such close neighbours, it is possible to detect a neutral fraction with a sensitivity similar to counts-in-cells measurements. If the two methods are combined, a neutral fraction as small as 10 per cent may be detectable at $z = 6.5$ using HSC.

In this more optimistic case, it may also become possible to use the Ly α EWs to directly map the locations, sizes and shapes of the largest ionized regions. Regardless of the availability of data, such bubble mapping is of course only possible if there actually is a substantial amount of neutral hydrogen at $z = 6.5$. In most reionization simulations, at an ionized fraction somewhere around 70 per cent or so, the ionized bubbles are overlapping to such a large extent that one can no longer speak of individual ionized regions. Additionally, we have seen that the feasibility of a bubble mapping measurement depends strongly on the intrinsic EW distribution—if there is a large amount of random scatter in the EWs, the correlation between local ionized fraction and observed EW is weak. If, however, such a bubble mapping measurement could be made, it could give unique insights into the topology of reionization. It would also provide great synergies with upcoming 21-cm experiments such as LOFAR and the SKA, for example for cross-correlating the Ly α emitter density with the 21-cm signal (Wiersma et al. 2013).

We have also investigated the prospects for using the JWST to constrain the IGM ionization state. The statistical methods we used to look for clustering in the HSC data do not work very well for the type of data produced by a deep spectroscopic survey. First of all, the sample size will be considerably smaller than for the HSC, even for a very ambitious survey. Second, such a survey will contain objects from a wide range of redshifts, so that any effect from an increasingly neutral IGM will be mixed up with whatever intrinsic galaxy evolution effects are present.

Nevertheless, we have shown that there is a chance that such a survey will detect a group containing a large number of galaxies in a small redshift interval at high z . Finding such a group would be a strong indication of a neutral IGM where galaxies reside in ionized bubbles, especially if the group contains one or more high-EW objects. However, even a detection like this would not be a conclusive proof of a neutral IGM, since similar groups can occur also in the other evolution scenarios considered here, albeit with much lower probability.

It is also interesting to compare our simulations to the recent observations by Pentericci et al. (2014) and Tilvi et al. (2014), who

performed spectroscopic observations of Ly α emitters at $z > 6$ and both found that the EW distribution at high redshifts is better explained by a patchy evolution model—where some objects are completely turned off and some are left as is—than a smooth model, where all galaxies are dimmed by a constant factor. The patchy model is intended as a toy model of reionization, where galaxies are either inside or outside ionized bubbles. However, in our simulations, galaxies are always located inside ionized bubbles, and the distribution of IGM transmission fractions, T_α , is not bimodal. The same result is found in most similar simulations (see e.g. McQuinn et al. (2007a) and Dijkstra, Mesinger & Wyithe 2011). With a unimodal T_α distribution, the EW distribution looks almost indistinguishable from the smooth evolution model, but very different from the patchy evolution model.

Interestingly, this implies that the results of Pentericci et al. (2014) and Tilvi et al. (2014) actually argue *against* the reionization scenarios produced by most simulations. It is not obvious what kind of scenario could produce the observed results, which show a strong deficit of intermediate-EW objects. It is conceivable that a situation like this could be produced in a scenario like that proposed by Bolton & Haehnelt (2013), in which the IGM at high z is highly ionized, but Ly α emitters are obscured by small, high-density clumps of neutral gas. If there are relatively few clumps, there could be some galaxies that are unobscured and others that are hidden behind clumps, leading to a bimodal T_α distribution. It is also possible that some change in the intrinsic properties of galaxies (such as evolution in the escape fraction; Dijkstra et al. 2014) is strong in some group of galaxies, and weak in the rest. Observations with the JWST will provide much better statistics on the EW distribution of high- z Ly α emitters. Regardless of whether the results of Pentericci et al. (2014) and Tilvi et al. (2014) are verified or not, this will teach us something about the evolution of galaxies in the early Universe.

While our results overall look rather promising, at least for the HSC, there are a few caveats to bear in mind. First, the observations we are considering are all very challenging, and some of our assumptions about them are somewhat optimistic. For example, obtaining UV luminosities for all the objects in the HSC survey may not be possible. Second, there are a number of uncertain parameters in our model for Ly α emitters, as discussed in more detail in section 3.1. Performing accurate simulations of Ly α production and radiative transfer through the circum- and intergalactic medium is a highly challenging task with many pitfalls. Our aim in this study has been to investigate the types of measurements that may become possible with the next generation of Ly α emitter surveys, rather than to explore every possible model uncertainty. We have therefore attempted to construct a model with reasonable assumptions that tend to lie on the conservative side.

In any case, the results from the next generation of Ly α emitter surveys will doubtless be of great value for studying reionization, regardless of what is actually observed. If a clustering signal can be seen in the HSC observations at $z = 6.5$, this will be strong evidence that reionization was still ongoing at this redshift. Conversely, if no clustering is seen, this will indicate that reionization is already almost completely finished by this redshift, and instead the intrinsic properties of Ly α change rapidly between $z = 6$ and $z = 6.5$. For the JWST, if a large group of galaxies could be detected at high redshift, this would be a strong indication of a partially neutral IGM. However, even without such luck, a deep spectroscopic survey with the JWST would put unprecedented constraints on the evolution of the EW distribution, which contains valuable information about the first galaxies in the Universe.

ACKNOWLEDGEMENTS

G.M. is supported in part by Swedish Research Council grant 2012-4144. E.Z. acknowledges research funding from the Swedish Research Council, the Swedish National Space Board and the Wenner-Gren Foundations. The authors thank Paul Shapiro and Kyungjin Ahn for the use of the 425/h Mpc reionization simulation results. Those results were obtained in part through an allocation of advanced computing resources provided by the National Science Foundation (P.I. P. R. Shapiro) at TACC and the National Institute for Computational Sciences (NICS), and in part at the GPC supercomputer at the SciNet HPC Consortium. SciNet is funded by: the Canada Foundation for Innovation under the auspices of Compute Canada; the Government of Ontario; Ontario Research Fund Research Excellence; and the University of Toronto. PL acknowledges support from the ERC-StG grant EGG5-278202. The Dark Cosmology Centre is funded by the D NRF. We are grateful to Masami Ouchi for useful discussions and for providing the expected number densities for the HSC survey, and to James Rhoads for valuable suggestions.

REFERENCES

- Adelberger K. L., Steidel C. C., Giavalisco M., Dickinson M., Pettini M., Kellogg M., 1998, *ApJ*, 505, 18
- Bish H., Vargas C. J., Gawiser E. J., Acquaviva V., Finkelstein S. L., 2013, in *American Astronomical Society Meeting Abstracts*, Vol. 221, American Astronomical Society Meeting Abstracts, p. 147.32
- Bolton J. S., Haehnelt M. G., 2013, *MNRAS*, 429, 1695
- Bouwens R. J., Illingworth G. D., Franx M., Ford H., 2007, *ApJ*, 670, 928
- Bouwens R. J. et al., 2011, *ApJ*, 737, 90
- Caruana J., Bunker A. J., Wilkins S. M., Stanway E. R., Lorenzoni S., Jarvis M. J., Elbert H., 2013, *ArXiv e-prints* 1311.0057
- Dayal P., Ferrara A., 2011, *MNRAS*, 417, L41
- Dijkstra M., Mesinger A., Wyithe J. S. B., 2011, *MNRAS*, 414, 2139
- Dijkstra M., Wyithe S., Haiman Z., Mesinger A., Pentericci L., 2014, *MNRAS*, 440, 3309
- Faisst A. L., Capak P., Carollo C. M., Scarlata C., Scoville N., 2014, *ApJ*, 788, 87
- Fan X. et al., 2006, *Astron. J.*, 132, 117
- Friedrich M. M., Mellema G., Alvarez M. A., Shapiro P. R., Iliev I. T., 2011, *MNRAS*, 413, 1353
- Guaita L. et al., 2011, *ApJ*, 733, 114
- Harnois-Déraps J., Pen U.-L., Iliev I. T., Merz H., Emberson J. D., Desjacques V., 2013, *MNRAS*, 436, 540
- Hayes M. et al., 2014, *ApJ*, 782, 6
- Hinshaw G. et al., 2013, *ApJS*, 208, 19
- Hu E. M., Cowie L. L., Barger A. J., Capak P., Kakazu Y., Trouille L., 2010, *ApJ*, 725, 394
- Hu E. M., Cowie L. L., McMahon R. G., Capak P., Iwamuro F., Kneib J.-P., Maihara T., Motohara K., 2002, *ApJL*, 568, L75
- Hutter A., Dayal P., Partl A. M., Müller V., 2014, *MNRAS*, 441, 2861
- Iliev I. T., Mellema G., Ahn K., Shapiro P. R., Mao Y., Pen U.-L., 2014, *MNRAS*
- Iliev I. T., Mellema G., Shapiro P. R., Pen U.-L., 2007, *MNRAS*, 376, 534
- Iliev I. T., Mellema G., Shapiro P. R., Pen U.-L., Mao Y., Koda J., Ahn K., 2012, *MNRAS*, 423, 2222
- Iliev I. T., Shapiro P. R., Mellema G., Merz H., Pen U.-L., 2008, in *Proceedings of the TeraGrid 2008 Conference*. June 9-13, 2008. Las Vegas, USA., p.31, pp. 31–
- Jensen H., Laursen P., Mellema G., Iliev I. T., Sommer-Larsen J., Shapiro P. R., 2013, *MNRAS*, 428, 1366
- Jiang L. et al., 2013, *ApJ*, 772, 99
- Kashikawa N. et al., 2011, *ApJ*, 734, 119
- Komatsu E. et al., 2011, *ApJS*, 192, 18

- Larson D. et al., 2011, *ApJS*, 192, 16
- Laursen P., Razoumov A. O., Sommer-Larsen J., 2009, *ApJ*, 696, 853
- Laursen P., Sommer-Larsen J., Razoumov A. O., 2011, *ApJ*, 728, 52
- Malhotra S., Rhoads J. E., 2004, *ApJL*, 617, L5
- McQuinn M., Hernquist L., Zaldarriaga M., Dutta S., 2007a, *MNRAS*, 381, 75
- McQuinn M., Lidz A., Zahn O., Dutta S., Hernquist L., Zaldarriaga M., 2007b, *MNRAS*, 377, 1043
- Mellema G., Iliev I. T., Alvarez M. A., Shapiro P. R., 2006, *New Astron.*, 11, 374
- Merz H., Pen U.-L., Trac H., 2005, *New Astron.*, 10, 393
- Mesinger A., Furlanetto S. R., 2008, *MNRAS*, 386, 1990
- Mitra S., Choudhury T. R., Ferrara A., 2012, *MNRAS*, 419, 1480
- Nilsson K. K., Tapken C., Møller P., Freudling W., Fynbo J. P. U., Meisenheimer K., Laursen P., Östlin G., 2009, *A&A*, 498, 13
- Ota K. et al., 2008, *ApJ*, 677, 12
- Ouchi M. et al., 2010, *ApJ*, 723, 869
- Pentericci L. et al., 2011, *ApJ*, 743, 132
- Pentericci L. et al., 2014, *ArXiv e-prints* 1403.5466
- Raskutti S., Bolton J. S., Wyithe J. S. B., Becker G. D., 2012, *MNRAS*, 421, 1969
- Reddy N. A., Steidel C. C., 2009, *ApJ*, 692, 778
- Schenker M. A., Stark D. P., Ellis R. S., Robertson B. E., Dunlop J. S., McLure R. J., Kneib J.-P., Richard J., 2012, *ApJ*, 744, 179
- Songaila A., 2004, *Astron. J.*, 127, 2598
- Stark D. P., Ellis R. S., Chiu K., Ouchi M., Bunker A., 2010, *MNRAS*, 408, 1628
- Stark D. P., Ellis R. S., Ouchi M., 2011, *ApJL*, 728, L2
- Taylor J., Lidz A., 2014, *MNRAS*, 437, 2542
- Theuns T., Zaroubi S., Kim T.-S., Tzanavaris P., Carswell R. F., 2002, *MNRAS*, 332, 367
- Tilvi V. et al., 2014, *ArXiv e-prints*
- Tilvi V. et al., 2010, *ApJ*, 721, 1853
- Treu T., Schmidt K. B., Trenti M., Bradley L. D., Stiavelli M., 2013, *ApJL*, 775, L29
- Treu T., Trenti M., Stiavelli M., Auger M. W., Bradley L. D., 2012, *ApJ*, 747, 27
- Verhamme A., Schaerer D., Maselli A., 2006, *A&A*, 460, 397
- Wiersma R. P. C. et al., 2013, *MNRAS*, 432, 2615
- Zackrisson E., Inoue A. K., Jensen H., 2013, *ApJ*, 777, 39
- Zheng Z.-Y., Wang J.-X., Malhotra S., Rhoads J. E., Finkelstein S. L., Finkelstein K., 2014, *MNRAS*